A Robust Control Framework for Smart Actuators[1]

Xiaobo Tan and John S. Baras
Institute for Systems Research and
Department of Electrical and Computer Engineering
University of Maryland, College Park, MD 20742 USA
{xbtan, baras}@isr.umd.edu

Abstract

Hysteresis in smart actuators presents a challenge in control of these actuators. A fundamental idea to cope with hysteresis is inverse compensation. But due to the open loop nature of inverse compensation, its performance is susceptible to model uncertainties and to errors introduced by inverse schemes. In this paper we develop a robust control framework for smart actuators by combining inverse control with the l_1 robust control theory, where the inversion error is modeled as an exogenous disturbance with a magnitude bound quantifiable in terms of parameter uncertainties and inversion schemes. Through the example of controlling a magnetostrictive actuator, we present a systematic controller design method which guarantees robust stability and robust trajectory tracking while taking actuator saturation into account. Simulation and experimental results are provided.

1 Introduction

Smart materials, such as magnetostrictives, piezoelectrics, shape memory alloys (SMAs), and magnetorheological (MR) fluids, all display certain coupling phenomena between applied electromagnetic/thermal fields and their mechanical/rheological properties. Smart actuators and sensors made of these materials have been receiving tremendous interest due to their broad applications in areas of aerospace, manufacturing, defense, and civil infrastructure systems, to name a few. The hysteretic behavior widely existing in smart materials, however, makes the effective use of these actuators and sensors quite challenging.

Models for smart actuators that capture both hysteresis and dynamic behaviour have a cascaded structure as shown in Figure 1(a) [1], where W is a hysteretic operator (with possibly some other nonlinearities) and $\hat{G}_a(\lambda)$ is a linear system. In this paper we consider the discrete-time setting in the interest of digital control, and $\hat{G}(\lambda)$ denotes the λ-transform of a linear time-invariant (LTI) system G. We recall that the λ-transform $\hat{G}(\lambda)$ is just the usual z-transform of G with $\lambda = z^{-1}$ [2].

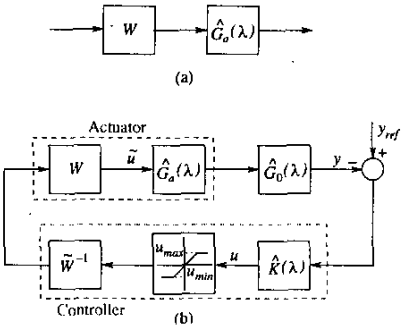

Figure 1: (a) The model structure for smart actuators; (b) The closed-loop system incorporating inverse compensation.

In Figure 1(b), $\hat{G}_0(\lambda)$ denotes the plant to be controlled by the actuator. A basic approach to cope with the hysteresis is to design an (approximate) right inverse operator $\tilde{W}^{-1}$ for W, then $\tilde{u} \approx u$ and the controller design problem is reduced to designing a linear controller $\hat{K}(\lambda)$ for the composite linear system $\hat{G}_0(\lambda) \circ \hat{G}_a(\lambda)$. The idea of inverse compensation can be found in, e.g., [3, 4, 5, 6, 7].

The most popular hysteresis model used in control of smart actuators has been the Preisach operator [3, 8, 7, 9]. The Preisach operator provides a means of developing phenomenological models that are capable of producing behaviors similar to those of physical systems. For a detailed treatment of the Preisach operator, we refer to [10, 11].

Due to the open loop nature of inverse compensation, its performance is susceptible to model uncertainties and to errors introduced by inversion schemes. To combat this problem, adaptive inverse control schemes were proposed for a class of hysteresis nonlinearities with parameterizable inverses [4]. For the Preisach operator-based hysteresis models, however, their inverses are not parameterizable in general. In this paper we develop a robust control framework for smart actuators by combining inverse control with the l_1 control techniques.

[1]This research was supported by the Army Research Office under the ODDR&E MURI97 Program Grant No. DAAG55-97-1-0114 to the Center for Dynamics and Control of Smart Structures (through Harvard University).

The inversion error is modeled as an exogenous disturbance with a magnitude bound quantifiable in terms of parameter uncertainties and inversion schemes. The design requirements for the controller $\hat{K}(\lambda)$ can be roughly stated as: in the presence of the inversion error and the uncertainties in $\hat{G}_a$ and $\hat{G}_0$, for all desired trajectories in a certain class, a) the closed-loop system is stable, b) the tracking error is minimized, and c) the output of $\hat{K}$ does not exceed the saturation limits. We take the saturation constraint (a common nonlinearity for actuators) into account in the design of $\hat{K}$ to ensure that the overall system operates in the linear region and thus predictions based on the linear design are credible. The controller design method will be illustrated through the example of robust trajectory tracking of a magnetostrictive actuator.

The remainder of the paper is organized as follows. In Section 2 we introduce the Preisach operator and an identification scheme for the Preisach operator. In Section 3 we describe the model for a magnetostrictive actuator. We discuss quantification of bounds on inversion errors in Section 4. We then formulate the robust control problem in Section 5. Simulation and experimental results are provided in Section 6. Finally we conclude in Section 7.

2 The Preisach Model

For a pair of thresholds (β, α) with $\beta \leq \alpha$, consider a simple hysteretic element $\hat{\gamma}_{\beta,\alpha}[\cdot,\cdot]$, as illustrated in Figure 2. For $u \in C([0,T])$ and an initial configuration $\zeta \in \{-1, 1\}$, the function

$$v = \hat{\gamma}_{\beta,\alpha}[u, \zeta] : [0, T] \to \{-1, 1\}$$

is defined as follows [11]:

$$v(0) \triangleq \begin{cases} -1 & \text{if } u(0) \leq \beta \\ \zeta & \text{if } \beta < u(0) < \alpha \\ 1 & \text{if } u(0) \geq \alpha \end{cases},$$

and for $t \in (0, T]$,

$$v(t) \triangleq \begin{cases} v(0) & \text{if } X_t = \emptyset \\ -1 & \text{if } X_t \neq \emptyset \text{ and } u(\max X_t) = \beta \\ 1 & \text{if } X_t \neq \emptyset \text{ and } u(\max X_t) = \alpha \end{cases},$$

where $X_t \triangleq \{\tau \in (0, t] : u(\tau) = \beta \text{ or } \alpha\}$.

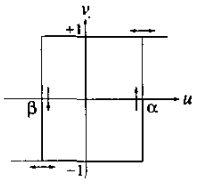

Figure 2: The elementary Preisach hysteron.

This operator is sometimes referred to as an *elementary Preisach hysteron* (we will call it a *hysteron* in this paper). The Preisach operator is a weighted superposition of all possible hysterons. Define

$$\mathcal{P}_0 \triangleq \{(\beta, \alpha) \in \mathbb{R}^2 : \beta \leq \alpha\}.$$

$\mathcal{P}_0$ is called the *Preisach plane*, and each $(\beta, \alpha) \in \mathcal{P}_0$ is identified with the hysteron $\hat{\gamma}_{\beta,\alpha}$. For $u \in C([0, T])$ and a Borel measurable initial configuration ζ_0 of all hysterons: $\zeta_0 : \mathcal{P}_0 \to \{-1, 1\}$, the output of the Preisach operator Γ is defined as [11]:

$$\Gamma[u, \zeta_0](t) = \int_{\mathcal{P}_0} \hat{\gamma}_{\beta,\alpha}[u, \zeta_0(\beta, \alpha)](t) d\nu(\beta, \alpha), \qquad (1)$$

where ν is a finite, signed Borel measure on $\mathcal{P}_0$, called the *Preisach measure.*

We call the Preisach measure ν *nonsingular* if $|\nu|$ is absolutely continuous with respect to the two-dimensional Lebesgue measure, and *singular* otherwise. By the Radon-Nikodym theorem, if ν is nonsingular, there exists a Borel measurable function μ, such that

$$\Gamma[u, \zeta_0](t) = \int_{\mathcal{P}_0} \mu(\beta, \alpha) \hat{\gamma}_{\beta,\alpha}[u, \zeta_0(\beta, \alpha)](t) d\beta d\alpha. \quad (2)$$

The weighting function μ is often referred to as the *Preisach function* or the *density function.* To simplify the discussion, throughout the paper we assume that μ has a compact support, $\mu(\beta, \alpha) = 0$ if $\beta < -r_0$ or $\alpha > r_0$ for some $r_0 > 0$. This leads us to consider $\mathcal{P} \triangleq \{(\beta, \alpha) \in \mathbb{R}^2 | \alpha \geq \beta, \beta \geq -r_0, \alpha \leq r_0\}$. At time t, $\mathcal{P}$ can be divided into two regions:

$$\mathcal{P}_{\pm}(t) \triangleq \{(\beta, \alpha) \in \mathcal{P} | \text{ output of } \hat{\gamma}_{\beta,\alpha} \text{ at } t \text{ is } \pm 1\}.$$

In most cases of interest, each of $\mathcal{P}_-$ and $\mathcal{P}_+$ is a connected set [10], and the output of Γ is determined by the boundary between $\mathcal{P}_-$ and $\mathcal{P}_+$ if the Preisach measure is nonsingular. The boundary is also called the *memory curve.* The memory curve has a staircase structure and its intersection with the line $\alpha = \beta$ gives the current input value. The memory curve ψ_0 at $t = 0$ is called the *initial memory curve* and it represents the initial condition of the Preisach operator.

If the Preisach measure is nonsingular, we can identify a configuration of hysterons ζ_ψ with a memory curve ψ in the following way: $\zeta_\psi(\beta, \alpha) = 1$ (-1, resp.) if (β, α) is below (above, resp.) the graph of ψ. Note that it does not matter whether ζ_ψ takes 1 or -1 on the graph of ψ. In the sequel we will put the initial memory curve ψ_0 as the second argument of Γ, where $\Gamma[\cdot, \psi_0] \triangleq \Gamma[\cdot, \zeta_{\psi_0}]$.

A constrained least squares scheme was proposed to identify the Preisach measure in [7]. In the scheme, the input is discretized into $L+1$ levels for some $L > 0$

Proceedings of the American Control Conference
Denver, Colorado June 4-6, 2003

and that leads to a discretized Preisach operator (Figure 3), i.e., a weighted sum of finitely many hysterons. What is identified in [7], is a collection of weighting masses sitting at centers of cells in the discretization grid (see the dark dots in Figure 3), which forms a singular Preisach measure. We can then obtain a non-singular approximation ν_p to the true Preisach measure ν by assuming each identified mass is distributed uniformly over the corresponding cell. Note that the density μ_p corresponding to ν_p is piecewise uniform.

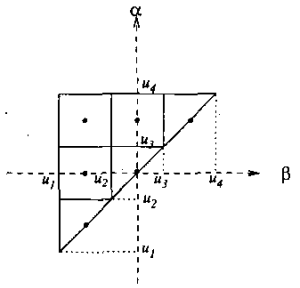

Figure 3: Discretization of the Preisach plane ($L = 3$).

3 The Model for Magnetostrictive Actuators

Magnetostriction is the phenomenon of strong coupling between magnetic properties and mechanical properties of some ferromagnetic materials (e.g., Terfenol-D). Figure 4 shows a sectional view of a Terfenol-D actuator. By varying the current in the coil, we vary the magnetic field in the Terfenol-D rod and thus control the displacement of the rod head.

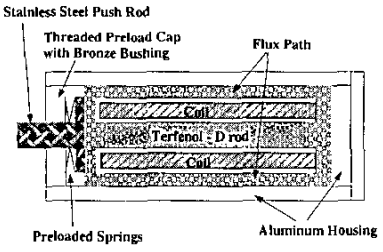

Figure 4: Sectional view of a Terfenol-D actuator [12](Original source: Etrema Products, Inc.).

When the input frequency is low (typically below 5 Hz), the magnetostrictive hysteresis is rate-independent: roughly speaking, the shape of the hysteresis loop is independent of the input frequency, and a model for the actuator is [7]:

$$\begin{cases} H(t) = c_0 I(t) \\ M(t) = \Gamma[H(\cdot), \psi_0](t) \\ y(t) = c_M M^2(t) \end{cases}, \qquad (3)$$

where I is the input current, y is the displacement of the actuator head, M and H are the bulk magnetization and the magnetic field (assumed uniform) along the rod direction, respectively, Γ is the Preisach operator, and c_0 and c_M are positive constants.

When the input frequency gets high, the magnetostrictive hysteresis is rate-dependent. A bulk magnetostrictive hysteresis model was proposed based on energy balancing principles in [12]. The model has a cascaded structure as shown in Figure 5. Note the resemblance of Figure 5 with Figure 1(a). $\bar{W}$ takes care of the M - H hysteresis and the eddy current losses, and the magnetoelastic dynamics of the rod is lumped into a second order linear system $G(s)$. $G(s)$ has a state space representation [12](after some manipulations):

$$\ddot{y}(t) + 2\xi\omega_0\dot{y}(t) + \omega_0^2 y(t) = \omega_0^2 c_M M^2(t), \qquad (4)$$

where ω_0 and ξ are positive constants.

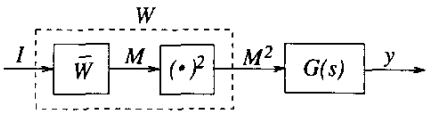

Figure 5: Model structure of a magnetostrictive actuator.

By replacing the switching ODE model in [12] with a Preisach operator Γ for the M - H hysteresis, we have proposed a new dynamic model [13, 14] for the $\bar{W}$ block:

$$\begin{cases} \dot{H}(t) + \dot{M}(t) = c_1(I(t) - \frac{H(t)}{c_0}) \\ M(t) = \Gamma[H(\cdot), \psi_0](t) \end{cases}, \qquad (5)$$

where c_1 is a positive constant.

Remark 3.1 *A variety of smart actuators have been modeled by essentially the Preisach operator alone as (3), e.g., see [3, 8]. On the other hand, the rate-dependent model (4) and (5) captures important dynamic effects in the frequency region of practical interest. Choosing the magnetostrictive actuator as the example allows us to cover both the rate-independent case and the rate-dependent case.*

4 Quantification of the Inversion Error

Recall Figure 1(b). For the Preisach operator-based W, there exists no stable Δ such that the inversion error $e_u = \tilde{u} - u$ can be modeled as $\Delta \cdot u$. Hence we model e_u as an exogenous disturbance. The inversion error is bounded in magnitude instead of in energy. Hence a natural choice for the signal spaces is l_∞ and not l_2. Also it is more appropriate to use l_∞ for the desired trajectory and the tracking error. Another advantage of using l_∞ for signals is that the actuator saturation constraint can be easily handled in the corresponding l_1 robust control theory, while it's very hard to be formulated in the $\mathcal{H}_\infty$ control theory.

We now quantify the error bounds in inversion of the Preisach operator and the dynamic model (5). Here

we are concerned with $e_M = \tilde{M} - M$, where $\tilde{M}$ and M denote the trajectories of achieved magnetization and desired magnetization, respectively. The bound on e_u when the square nonlinearity in Figure 5 is included can be easily derived from the bound on e_M.

4.1 Inversion of the Preisach operator Γ

If the Preisach measure ν is given, an iterative inversion algorithm is available and $\|e_M\|_\infty \leq \epsilon$, where ϵ is the stopping criterion [13]. If ν is unknown, we can obtain a nonsingular approximation ν_p with a piecewise uniform density μ_p as discussed in Section 2. The Preisach operator with measure ν_p can be inverted exactly (in a finite number of steps) [13]. Hence the inversion error e_M is solely due to the measure error $|\nu - \nu_p|$. It turns out that we can quantify the error bound in terms of the relative error of identification and the discretization level L of the Preisach plane:

Proposition 4.1 *[13] Let the true Preisach measure ν be nonnegative and nonsingular with density $\mu \leq \bar{\mu}$, where $\bar{\mu} > 0$ is a constant. Given a discretization of level L, denote ν_i^0 the integral of μ over the i-th cell, and ν_i the identified mass for the same cell. Assume $\frac{|\nu_i - \nu_i^0|}{\nu_i^0} \leq \delta_I$, $\forall i$, where $\delta_I > 0$ is some constant. Then*

$$\|e_M\|_\infty \leq \delta_I M_s + \frac{8\bar{\mu} r_0^2}{L},$$

where M_s is the positive saturation corresponding to ν.

4.2 Inversion of (5)

An inversion scheme was proposed for the model (5) [14]. But if there is uncertainty in the model parameters, it is very hard to derive a bound for the inversion error. We now present another inversion algorithm. Eq. (5) can be rewritten as:

$$\begin{cases} \dot{H}(t) = \frac{c_1}{1+g(t)}(I(t) - \frac{H(t)}{c_0}) \\ M(t) = \Gamma[H(\cdot), \psi_0](t) \end{cases}, \tag{6}$$

where $g(t)$ carries the interpretation of "$\frac{dM}{dH}$" at time t, and it depends on both the state ψ_t (the memory curve at t) and the sign of $\dot{H}$ [13]. Under mild conditions, $0 \leq g(t) \leq C$ for some $C > 0$. We can view (6) as perturbed from the following decoupled system:

$$\begin{cases} \dot{H}(t) = \frac{c_1}{1+\bar{g}}(I(t) - \frac{H(t)}{c_0}) \\ M(t) = \Gamma[H(\cdot), \psi_0](t) \end{cases}, \tag{7}$$

where $\bar{g} \in [0, C]$ is some constant. Based on (7), an *approximate* inversion scheme for (6) is given formally by

$$\begin{cases} H(t) = \Gamma^{-1}[M(\cdot), \psi_0](t) \\ I(t) = \frac{1+\bar{g}}{c_1}\dot{H}(t) + \frac{H(t)}{c_0} \end{cases}. \tag{8}$$

In the discrete-time implementation, a delay is introduced in the inversion due to the dynamics. Hence the inversion error is defined as $e_M[k] \triangleq \tilde{M}[k] - M[k-1]$. We can choose an explicit or implicit Euler scheme in discretizing (5) and (8), and for either scheme, we can quantify the error bound in terms of model parameters, see [13].

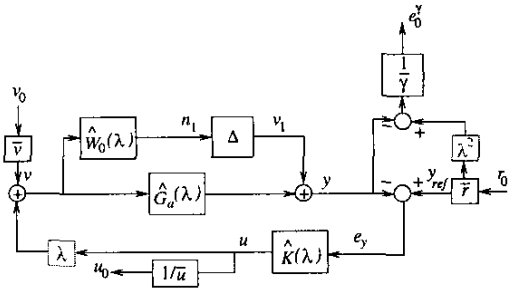

Figure 6: Robust control of a magnetostrictive actuator.

Remark 4.1 *The inversion algorithm (8) leads to an inversion error even if the exact parameters are known. But the payoff is that, this scheme allows us to quantify the inversion error when parameter errors are present.*

5 Formulation of the Robust Control Problem

In this paper, we consider $\hat{G}_0(\lambda)$ to be the identity operator, i.e., we are interested in trajectory tracking of the actuator head itself. Figure 6 shows the closed-loop system after the inverse compensation is done, where the exogenous noise v represents the inversion error. From the previous section, $\|v\|_\infty \leq \bar{v}$, and $\bar{v}$ is quantifiable in terms of inverse schemes and parametric uncertainties. The composition $\Delta \circ \hat{W}_0(\lambda)$ represents the deviation of the actual plant from the nominal plant $\hat{G}_a(\lambda)$. We assume that Δ can be any nonlinear operator with $\|\Delta\|_{l_\infty - ind} < 1$. $\hat{W}_0(\lambda)$ is a weighting function and it reflects that the model uncertainty is larger at a higher frequency.

Let $\|y_{ref}\|_\infty \leq \bar{r}$, where y_{ref} is the reference trajectory. The error $e_y \triangleq y_{ref} - y$ is fed into the controller $\hat{K}(\lambda)$. The delay λ following $\hat{K}(\lambda)$ is due to inversion of the dynamic hysteresis model. Let the saturation limits of the actuator be $-\bar{u}$ and $\bar{u}$ respectively. Then the saturation constraint translates into $\|u_0\|_\infty \leq 1$, where u_0 is as defined in Figure 6. The case $u_{min} \neq -u_{max}$ can be handled by defining $\bar{u} = \frac{u_{max} - u_{min}}{2}$ and $u_b = \frac{u_{max} + u_{min}}{2}$, where u_b is a bias input to be injected into the system [13].

There are two delays in the loop since $\hat{G}_a(\lambda)$ contains a pure delay. This motivates us to define the tracking error e_0^γ as

$$e_0^\gamma[k] \triangleq \frac{y_{ref}[k-2] - y[k]}{\gamma}, \tag{9}$$

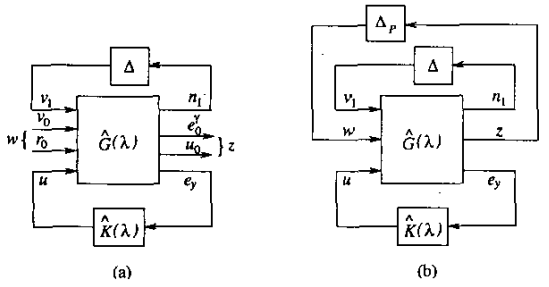

Figure 7: Formulation of the robust control problem.

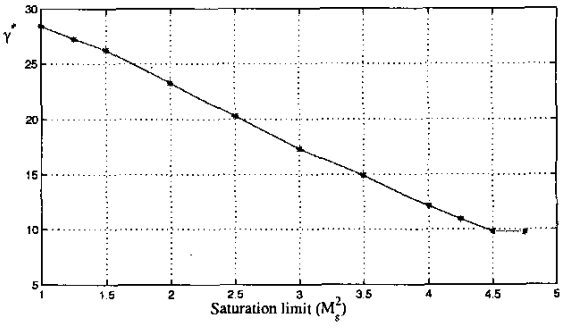

Figure 8: Effect of the saturation limit on γ^*.

where $\gamma > 0$ is called *the disturbance attenuation level.* To ease the formulation, we normalize signals v and y_{ref}, and regard v_0 and r_0 as inputs to the system with $\|v_0\|_\infty \leq 1$, $\| r_0 \|_\infty \leq 1$ (Figure 6). The transfer function $\hat{G}(\lambda)$ from $(v_1, v_0, r_0, u)^T$ to $(n_1, e_0^\gamma, u_0, e_y)^T$ can be easily written down. In terms of $\hat{G}$, the closed-loop system in Figure 6 can be simplified as in Figure 7(a).

The control objective is to find the smallest γ and a stabilizing controller $\hat{K}(\lambda)$, such that

1. the closed-loop system is stable for any Δ with $\|\Delta\|_{l_\infty - ind} < 1$,
2. $\|e_0^\gamma\|_\infty \leq 1$ if $\Delta = 0$, $\forall v_0$, r_0 with $\|v_0\|_\infty \leq 1$ and $\|r_0\|_\infty \leq 1$, and
3. $\|u_0\|_\infty \leq 1$ if $\Delta = 0$, $\forall v_0$, r_0 with $\|v_0\|_\infty \leq 1$ and $\|r_0\|_\infty \leq 1$.

If we define the exogenous input w and the regulated output z as shown in Figure 7(a), items 2 and 3 above translate into $\|\Phi_{zw}\|_1 \leq 1$, where Φ_{zw} denotes the transfer function from w to z, and $\| \cdot \|_1$ denotes the l_1 norm of an LTI system. By the small gain theorem, this is equivalent to requiring robust stability of the system when we wrap a nonlinear uncertainty block Δ_P from z to w with $\|\Delta_P\|_{l_\infty - ind} < 1$ (Figure 7(b)).

Now the control problem can be reformulated as: find the smallest γ and a stabilizing controller $\hat{K}(\lambda)$, such that the closed-loop system in Figure 7 (b) is robustly stable for all $\tilde{\Delta} \in \tilde{\mathbf{\Delta}}$, where $\tilde{\mathbf{\Delta}} \triangleq \{\tilde{\Delta} = diag(\Delta, \Delta_P) :$ Δ is nonlinear and of dimension 1×1, Δ_P is nonlinear and of dimension 2×2, $\|\tilde{\Delta}\|_{l_\infty - ind} < 1\}$. The procedures to solve this problem can be found in [2].

6 Simulation and Experimental Results

6.1 Effects of design parameters on γ^*

We first present computation results on how the optimal attenuation level γ^* is affected by the design parameters. For the sampling frequency 2000 Hz, $\hat{G}_a(\lambda) = \frac{2.23\times10^{-11}\lambda^2 + 4.28\times10^{-11}\lambda}{0.147\lambda^2 - 0.549\lambda + 1}$ based on the identified parameters. We let $\hat{W}_0(\lambda) = \frac{1.1759 c_w (\lambda - 1.0005)}{\lambda - 1.1765}$, where $c_w > 0$ determines the magnitude of the uncertainty.

Figure 8 shows how γ^* varies with the saturation constraint $\bar{u}$. We have used $\bar{r} = 30$, $c_w = 6.53 \times 10^{-13}$, and $\bar{v} = 0.1 M_s^2$, where M_s is the saturation magnetization. Since the range of u for the magnetostrictive actuator is $[0, M_s^2]$, expressing $\bar{v}$ and $\bar{u}$ in terms of M_s^2 allows one to make more concrete sense out of these numbers. From Figure 8, γ^* drops when $\bar{u}$ increases, but γ^* becomes a constant when $\bar{u}$ hits $4.5 M_s^2$, beyond which the saturation constraint no longer plays a role. Effects of c_w and $\bar{v}$ on γ^* have also been studied, and we find that γ^* drops as c_w or $\bar{v}$ does so [13].

6.2 Results of trajectory tracking

As we have seen from Figure 8, the tracking performance deteriorates as the saturation constraint $\bar{u}$ is tightened. For the magnetostrictive actuator, $\bar{u} = 0.5 M_s^2$ and strictly enforcing this constraint would lead to large tracking errors. This reveals the limitation of pure linear design for an intrinsically nonlinear plant. Hence a practical approach would be to properly relax the constraint.

Figure 9(a) shows the simulation result of tracking a sinusoidal signal. The current I applied is also displayed. The controller $\hat{K}(\lambda)$ is designed based on $c_w = 3.3 \times 10^{-13}$, $\bar{v} = 0.1 M_s^2$, and $\bar{u} = 3.25 M_s^2$. Although we set $\bar{u} = 3.25 M_s^2$ in the controller design, the control u stays in the (true) unsaturated region $[-0.5 M_s^2, 0.5 M_s^2]$ except during the transient period at the beginning [13]. Our composite controller (the linear robust controller plus the inverse algorithm) is compuation efficient and we can implement it in real-time. Figures 9(b) shows the experimental result of trajectory tracking based on the same controller as used in the simulation. It matches well with the simulation result and the overall performance is satisfactory. We have also performed simulation and experiment of tracking an irregular signal, and the results are similar to those in Figures 9(a) and 9(b) [13]. The saturation limit $\bar{u}$ can not be "over-relaxed". Experiments have shown

Proceedings of the American Control Conference
Denver, Colorado June 4-6, 2003

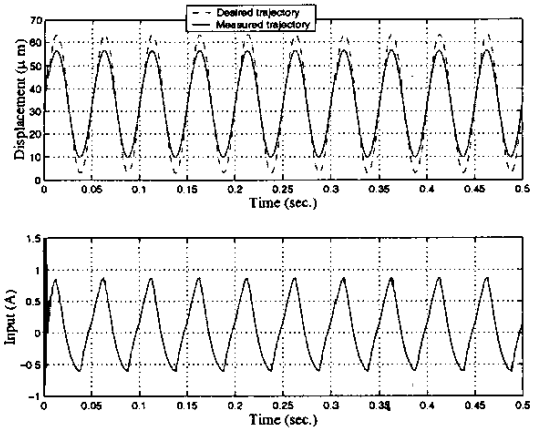

(a)

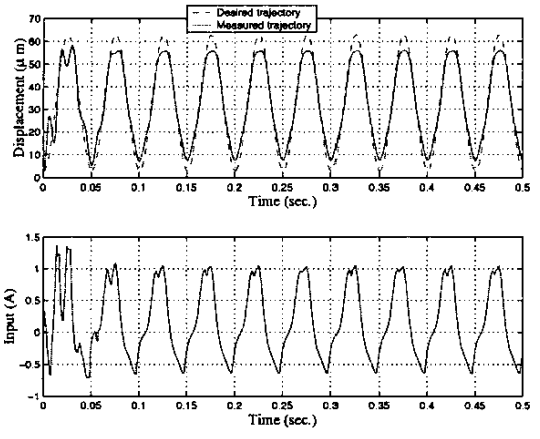

(b)

Figure 9: (a) Simulation result of trajectory tracking; (b) Experimental result of trajectory tracking.

that the tracking performance suffers from persistant control saturation if we set $\bar{u} = 5M_s^2$ in the design [13].

7 Conclusions

In this paper, we have presented a robust control framework for smart actuators by combining the inverse compensation with the linear robust control theory. We modeled the inversion error as an exogenous noise with a quantifiable bound on its magnitude. Robust control techniques were then employed to attenuate the impact of the inversion error as well as ensure stability in the presence of uncertainty. The saturation constraint was also incorporated into the controller design. Simulation and experimental results have demonstrated the effectiveness of the approach.

The first author would like to acknowledge useful discussions with Professors R. Venkataraman, P. S. Krishnaprasad, and A. Tits.

References

[1] R. Venkataraman and P. S. Krishnaprasad, "Approximate inversion of hysteresis: theory and numerical results," in *Proceedings of the 39th IEEE Conference on Decision and Control*, 2000, pp. 4448–4454.

[2] M. A. Dahleh and I. J. Diaz-Bobillo, *Control of Uncertain Systems: A Linear Programming Approach*, Prentice-Hall, Englewood Cliffs, NJ, 1995.

[3] D. Hughes and J. T. Wen, "Preisach modeling and compensation for smart material hysteresis," in *Active Materials and Smart Structures*, 1994, vol. 2427 of *SPIE*, pp. 50–64.

[4] G. Tao and P. V. Kokotović, "Adaptive control of plants with unknown hysteresis," *IEEE Transactions on Automatic Control*, vol. 40, no. 2, pp. 200–212, 1995.

[5] R. C. Smith, "Inverse compensation for hysteresis in magnetostrictive transducers," Tech. Rep. CRSC-TR98-36, CRSC, NC State, 1998.

[6] W. S. Galinaitis and R. C. Rogers, "Control of a hysteretic actuator using inverse hysteresis compensation," in *Mathematics and Control in Smart Structures*, 1998, vol. 3323 of *SPIE*, pp. 267–277.

[7] X. Tan, R. Venkataraman, and P. S. Krishnaprasad, "Control of hysteresis: theory and experimental results," in *Modeling, Signal Processing, and Control in Smart Structures*, 2001, vol. 4326 of *SPIE*, pp. 101–112.

[8] R. B. Gorbet, D. W. L. Wang, and K. A. Morris, "Preisach model identification of a two-wire SMA actuator," in *Proceedings of IEEE International Conference on Robotics and Automation*, 1998, pp. 2161–2167.

[9] D. Croft, G. Shed, and S. Devasia, "Creep, hysteresis, and vibration compensation for piezoactuators: atomic force microscopy application," *Journal of Dynamic Systems, Measurement, and Control*, vol. 123, no. 1, pp. 35–43, 2001.

[10] I. D. Mayergoyz, *Mathematical Models of Hysteresis*, Springer Verlag, 1991.

[11] A. Visintin, *Differential Models of Hysteresis*, Springer, 1994.

[12] R. Venkataraman, *Modeling and Adaptive Control of Magnetostrictive Actuators*, Ph.D. thesis, University of Maryland, College Park, 1999.

[13] X. Tan, *Control of Smart Actuators*, Ph.D. thesis, University of Maryland, College Park, MD, Sept. 2002, available online at `http://www.isr.umd.edu/TechReports/ISR/2002`, in the PhD Thesis section.

[14] X. Tan and J. S. Baras, "Modeling and control of a magnetostrictive actuator," in *the Proceedings of the 41st IEEE Conference on Decision and Control*, 2002, pp. 866–872.